Large-Eddy Simulation and Analysis of Tip-Clearance Flows in Turbomachinery Applications

Donghyun You
Stanford University
dyou@stanford.edu

Meng Wang
Stanford University
wangm@stanford.edu

Rajat Mittal
The George Washington University
mittal@seas.gwu.edu

Parviz Moin
Stanford University
moin@stanford.edu

Abstract

The tip-leakage flow in axial turbomachines is studied using large-eddy simulation with an emphasis on understanding the underlying mechanisms for low-pressure fluctuations and cavitation downstream of the tip-gap. Simulation results are validated against experimental measurements, and reasonable agreements are obtained. Dominant vortical structures such as the tip-leakage vortex and tip-separation vortices are examined, and their effects on the turbulent flow characteristics as well as on the low-pressure statistics are investigated. Analysis of the velocity and pressure fields suggests a high correlation between cavitation inception and the tip-leakage vortex. To suppress the tip-leakage vortex and the associated low-pressure events, the use of a grooved casing wall is explored, and preliminary simulation results show good promise. Additional simulations to investigate the effects of inflow vortices and tip-gap size are also discussed.

1. Introduction

In hydraulic turbomachines such as submarine propulsors and liquid fuel pumps, the existence of radial clearance between the rotor-blade tip and the casing wall has been a major source of cavitation, which can result in loud acoustic noise and performance deterioration. Although it is generally recognized that cavitation is associated with low-pressure fluctuations downstream of the tip-gap, the underlying mechanisms are not well understood. In order to gain insight into these mechanisms, it is necessary to study the detailed turbulence dynamics in the rotor-blade wake and the tip-clearance region. This understanding is also a necessary precursor to devising efficient cavitation-control methodologies.

Previous experimental studies[1-6] have revealed various qualitative and some quantitative features of the tip-clearance flow. In the recent experiments performed by Devenport's group at Virginia Tech, Muthanna[4,5] and Wang[6] made detailed measurements of the flow field downstream of rotor blades in a low speed linear compressor cascade employing stationary and moving endwalls. These experiments have provided useful information about the flow as well as valuable data for validating computational techniques. In recent years, researchers have also examined ways to alter the tip-leakage vortex and thereby diminish the negative effects of the tip-clearance flow. Kameier and Neise[3] performed an experiment employing a turbulence generator (plastic tape) attached to the blade-tip while Khorrami *et al.*[7] treated the rotor-tip with porous wall in their Reynolds-averaged Navier-Stokes (RANS) simulation. Casing wall modification is another common method for controlling the tip-leakage flow. For example, Bae *et al.*[8] devised synthetic jet actuators which are mounted on the casing endwall, and Crook *et al.*[9] used a grooved endwall in their numerical study.

The above experimental and RANS-based numerical studies have added significantly to our knowledge regarding the structure of the rotor tip-clearance flow. However, both these approaches are limited in their ability to provide data on the detailed dynamics and the resulting cavitation-inducing low-pressure events. In the present work, we use large-eddy simulation (LES) as a tool to study the tip-leakage flow, with the objective of gaining a deeper understanding of the unsteady flow characteristics. LES is quite suited for studying such flows since it has the capability of resolving the energy containing scales temporally as well as spatially.

The flow configuration considered is the same as in one of the VPI experiments,[6] which involves a linear cascade with tip-clearance and moving endwall. An accurate LES of this flow is very challenging due to the large mesh-size requirement, the fully three-dimensional nature of the simulation, and the need for statistical convergence and long-time sampling. Currently, we perform simulations with approximately 23 million grid points, and each simulation requires $O(10^5)$ single-processor CPU hours on SGI Origin 3800. The computational resources provided by DoD HPCMP through the Challenge Grant are one of the most crucial factors for the success of this study.

During the 2002-2003 period our research has focused on the following aspects: (i) validation of the LES against the VPI experiments[6] and accumulation of a flowfield database; (ii) detailed analysis of the database with an emphasis on understanding the turbulence characteristics, vortex dynamics and low-pressure fluctuations around the tip-gap region; (iii) study of the tip-gap size effect and interaction with incoming vortices; and (iv) investigation of tip-vortex control though passive shape modification. Progress is highlighted in the remainder of this section and discussed in detail in Sections 2 and 3.

To validate the LES solutions, a series of simulations have been performed to examine the effects of grid resolution and spanwise domain size. Earlier coarse-grid (8 million points) solutions were found to severely under-predict the size and strength of the tip-leakage vortex compared with the experiment, and the vortex location was also found incorrect. These problems have largely been rectified in the new fine-mesh (23 million points) simulation, which shows reasonably agreement with the experimental data.

The databases obtained are analyzed in order to elucidate the mechanisms responsible for low-pressure fluctuations and cavitation inception. It is in general difficult to accurately predict cavitation using single-phase CFD,[11,12] although a variety of cavitation-inception criteria have been developed.[12-14] In our analysis we use the one proposed by Joseph[13] which consists of the local pressure, vapor pressure as well as the tensile stress of the fluid. This criterion has found relatively wide support in literature.[11,14]

It is well known that the tip-gap size and inflow vortices have strong effects on the position, size and strength of the tip-leakage vortex,[4-6,10] To quantify the tip-gap size effects, two simulations, with one-half and twice the original tip-gap size, are currently underway, and preliminary results will be presented. We have also started a simulation of vortex generator interacting with a turbulent-boundary layer, which will provide the inflow data for the tip-clearance flow simulation with upstream vortex effect. The same configuration was used in a recent experiment at VPI.[10]

The ultimate goal of the present study is to find ways to reduce cavitation and the associated detrimental effects in the tip-leakage flow. As an initial attempt, the use of an endwall groove as a tip-leakage vortex reducer is being investigated using LES. The location and size of the groove are determined using the information obtained from LES with the untreated endwall.

Finally, an effort has been made to continuously improve the newly developed LES code in order to fully and efficiently utilize the DoD HPC resources, particularly new platforms such as the IBM Regatta P4.

2. Problem and Methodology

A. Numerical Method

The numerical algorithm and solution method are described in detail in Refs. 15-17. Here, we summarize the main features of the methodology.

The three-dimensional, unsteady, incompressible Navier-Stokes equations are solved in a generalized coordinate system in conjunction with a Smagorinsky type dynamic subgrid-scale (SGS) model. Given the fully inhomogeneous nature of the flow, it is necessary to implement a Lagrangian dynamic SGS model which averages the model coefficient along the flow pathlines.[18]

The integration method used to solve the governing equations is based on a fully-implicit fractional-step method which avoids the severe time-step restriction in the tip-clearance region. All terms including cross-derivative diffusion terms are advanced in time using the Crank-Nicolson method and are discretized in space by energy-conserving second-order central-differencing. A Newton iterative method is used to solve the discretized nonlinear equations. For the pressure Poisson equation, an efficient multigrid procedure, which is a combination of the line and red-black Gauss-Seidel multigrid method is used. This method is particularly appropriate for parallelization. Since the Poisson solver is the most expensive part of computation in this fully three-dimensional flow, it is crucial to improve both the convergence ratio and the parallel efficiency.

The simulation code is parallelized using OpenMP for various shared-memory parallel computers such as the SGI Origin 2000 and 3000 series, IBM Regatta P4 and Compaq GS320. A difficulty encountered with the large mesh-size simulation is the stack memory requirement which often exceeds the available amount on certain computer systems. Therefore, remedies such as dynamic memory allocation/deallocation and

stackable array splitting have been implemented to make the simulations feasible with minimum loss in parallel efficiency.

Figure 1 shows the parallel performance of the present LES code on various computer platforms. The code achieves close to linear scaleups on both SGI Origin 3800 and IBM Regatta P4. The limited stack-memory size is partly responsible for the lower scaleup on Compaq GS320.

B. Flow Configuration

The flow configuration and coordinate definition are schematically shown in Fig. 2. The present study is focused on a linear cascade with a moving endwall at the bottom of the tip gap, matching the experimental setup of Wang.[6] Only a single blade is considered, with periodic boundary conditions in the y-direction to mimic the flow in the interior of a cascade. The computational domain is of size $L_x \times L_y \times L_z = 1.6C \times 0.929C \times 0.5C$, where C is the blade chord. The mesh size used for the final simulation is $449 \times 351 \times 129$. It is determined iteratively based on the results from a number of coarser-mesh simulations.

The important parameters for the base simulation are as follows: The size of the tip-clearance is $0.0165C$, the blade pitch is $0.9C$, and the blade span is $0.5C$ ($1C$ in the experiments). The blade has a relatively high stagger-angle of about 57 degrees. The Reynolds number of this flow is 400,000 based on the chord and inflow free-stream velocity, and the inflow turbulent boundary layer has a Reynolds number of 780 based on the momentum thickness.

The inflow turbulent boundary-layer data is provided using the method of Lund et al.,[19] modified to account for the fact that the mean flow direction is not perpendicular to the inflow/outflow plane. No-slip boundary conditions are applied along the rotor blade and moving endwall and convective boundary condition is applied at the exit boundary.

The difficulty with grid topology in the tip-clearance region is overcome by a novel approach which combines an immersed boundary technique[20] with a structured grid in a generalized coordinate system. In addition to this, the high stagger angle in the experimental setup necessitates the use of very skewed mesh, which requires fine control of mesh parameters such as stretching ratio and aspect ratio, and an adequate formulation of nonlinear convection terms to avoid numerical instability (see Ref. 13 for more details).

3. Results

A. Flow-Field Validation

Comparisons of the flow fields have been made between the LES solutions and experimental measurements[6] at locations downstream of the rotor blade. In the experiment, four sets of hot wire measurements were taken to obtain detailed information about the mean and turbulent flow fields in planes 1 and 2 shown in figure 2(b).

The mean streamwise velocity from the LES is compared with experimental values in Figs. 3 and 4, at two measurement locations $x/Ca = 1.51$ and $x/Ca = 2.74$, respectively, as seen by an observer looking upstream. Here Ca ($= 0.546C$) is the axial chord length by which the locations are normalized. Vertical bundles of the mean streamwise velocity contours are present in the wakes of rotor blades, and the tip-leakage vortices are found near the endwall in both the simulation and the experiment.[6] Compared with the experimental findings, agreements are generally good, and remarkably better in the vortex size, strength, and its downstream position than the previous coarse-mesh LES solutions.[15] This illustrates that adequate grid resolution is crucial for capturing the evolution of vortical structures in the tip-leakage flow.

The tip-leakage flow and the blade wake are the main sources of turbulent fluctuations and energy. Reynolds stresses are compared with the experimental data[6] in Figs. 5 and 6. They again show reasonable agreements, notably in the regions dominated by the tip-leakage vortex and the wake. Furthermore, the present simulations have been shown to predict the experimental energy spectra over a wide range of frequencies without excessive numerical dissipation. More extensive validations including energy spectra and pressure distribution can be found in Ref. 17.

The statistical quantities presented here and in Section 3B are time-averaged over 7 flow-through times ($7C/U_\infty$). Before statistics are collected, the simulations have advanced 5 flow-through times to wash out the initial transients.

B. Vortex Structures and Low-Pressure Fluctuations

An examination of the flowfield indicates that the tip-leakage vortex plays a dominant role in the generation of turbulence and intense pressure fluctuations downstream of the tip-gap near the endwall. To better identify the vortical structures, the λ_2 vortex identification method[21] is used. Figure 7 shows typical vortical structures predicted by the present LES as visualized by the λ_2 iso-surfaces. The most dominant

vortical structure is the tip-leakage vortex which is generated near the blade leading-edge and convects downstream while expanding in size (A in Fig. 7). This is accompanied by counter-rotating vortical structures B, which are generated further upstream and terminated in the blade passage due to blockage by the neighboring blade. Small vortical structures abundant near the trailing-edge region (C in Fig. 7) are related to the tip-separation vortices. They are extremely complicated due to interaction with the tip-leakage vortex from the neighboring blade. As a result of the interaction, the tip-leakage vortex evolves into a bunch of small scale vortical structures. Similar observations have been reported by experiments.[4-6] This could explain the low-pressure events in the downstream endwall region.

Detailed statistics of negative pressure fluctuations have been collected and analyzed in order to study cavitation. Figure 8 shows contours of the time-averaged pressure (Fig. 8(a)) and root-mean square pressure fluctuations (Fig. 8(b)) in an *x-y* plane inside of tip-gap. The spatial and temporal variations of the negative pressure relative to the mean values appear to be highly correlated with the vortical structures in the tip-leakage flow, particularly in the tip-leakage and tip-separation vortices.[17]

The negative pressure regions are known to be susceptible to cavitation. Figure 9 shows an example of cavitation inception analysis using the minimum tension criterion proposed by Joseph.[13] This criterion is based on the normal stress of the fluid and the critical vapor pressure:

$$B_{ii} = \tau_{ii} - p + p_c > 0,$$

where τ_{ii} is the normal stress, p is local pressure and p_c is the pressure in the cavity. For this example, p_c of 0.01 is used, assuming the cavitation number of 0.02 based on the cascade inlet pressure. If all three components of the stress B_{11}, B_{22} and B_{33} are positive, a cavity will open. Similar discussions can be found in Knapp *et al.*[14]

Instantaneous and time-averaged contours of $B = 1/3(B_{11}+B_{22}+B_{33})$ are plotted in Figs. 9(a) and 9(b), respectively, in regions where all three components are positive. High levels of B in both the instantaneous and time-averaged contours are concentrated in the tip-leakage region. In particular, the tip-leakage vortex appears as the dominant source of cavitation. The tip-separation vortex is less important even though it involves equally low pressure (cf. Fig. 8). This is partially due to the high positive values of the normal stress τ_{ii} in addition to the strong negative pressure found in the tip-leakage vortex.

C. Effects of Tip-Gap Size and Vortex-Rotor Interaction

The tip-gap size relative to the chord is a key parameter for this flow. In order to evaluate its effect on the vortical structures and low-pressure characteristics, two simulations, with one-half ($0.00825C$) and twice ($0.033C$) the tip-gap size of the baseline case, are currently in progress. These same tip-gap sizes have also been considered in the experiments of Devenport's group.[6]

Figure 10 shows time-averaged pressure contours inside the tip-gaps at $z/Ca = 0.001$. Solutions for the half- and double-size cases have not fully converged due to the short sampling time ($1.5C/U_\infty$), yet a qualitative comparison can be made. Relative to the base tip-gap size (Fig. 10(a)), the increased tip-gap enhances both the size and strength of the tip-leakage vortex, thereby resulting in larger and more negative pressure regions around tip-leakage vortex (Fig. 10(b)). In contrast, as seen in Fig. 10(c), the smaller tip-gap reduces the tip-leakage vortex size while enhancing the tip-separation vortices.

Another issue of practical interest is the influence of large-scale vortices in the inflow, such as those in the stator wake. In a recent experiment at VPI[10] vortex generators are used to emulate the effect of the stator wake. We have initiated a corresponding numerical simulation involving a turbulent boundary layer interacting with a vortex generator, in a configuration schematically shown in Figure 11. The vortex generators in the experiment are of thin delta-wing shape, which is difficult to resolve using a conventional mesh topology. To overcome this difficulty, we again utilized the immersed boundary technique.

The feasibility of this methodology has been established in a low Reynolds number flow. Figure 12 plots an iso-surface of instantaneous pressure ($p/\rho U_\infty^2 = -0.02$), showing a convecting vortex-pair generated by the vortex generator. Currently, a simulation for the vortex generator in a turbulent boundary layer is underway. The results will be compared with the experiment at VPI.[10] The time series of the velocities downstream of the vortex generator will be saved and fed as inflow to the rotor tip-clearance flow simulation.

D. Control of Tip-Leakage Vortex

As indicated previously, the tip-leakage vortex is highly correlated with the turbulent and low-pressure fluctuations which are responsible for cavitation. Therefore, a control strategy for suppressing the tip-

leakage vortex is expected to also reduce or eliminate cavitation and the associated unfavorable effects.

To this end, we explored the use of an endwall groove as shown schematically in Figure 13. The location and size of the groove are preliminarily determined based on an analysis of the flow physics, and can be optimized iteratively. The groove introduces disturbances in the tip-gap region, which interacts with the tip-leakage flow, causing enhanced mixing and less coherent flow structures

Before this control strategy is applied to the full Reynolds number (Re = 400,000) case, we assessed its feasibility and efficiency at a lower Reynolds number of 10,000 with uniform inflow. These simplifications are partly justified by observing that the tip-leakage vortex in the tip-gap region is highly coherent and behaves like a laminar vortex even at the Reynolds number of 400,000.[16] The simulation setup is the same as in the uncontrolled baseline case, except that a stationary endwall and a $321 \times 261 \times 113$ mesh are used. The endwall groove is placed near the leading edge at $L_0 = 0.1$, which corresponds to the origin of tip-leakage vortex. The height, $H = 0.0165C$, is of the same size as the tip-gap, and the width $L = 3H$ (see Fig. 13 for the definitions of L_0, L and H).

Figure 14 shows preliminary results from the simulations of controlled and uncontrolled tip-leakage flows in terms of the instantaneous vorticity magnitude. These results appear promising in the sense that the tip-leakage vortex loses its coherence more rapidly in the grooved case compared to the un-grooved one.

It should be pointed out that the use of an endwall groove can have adverse effects on drag, pressure rise, as well as acoustics and vibration issues. However, these effects can be mitigated by choosing an appropriate combination of groove parameters and tip-gap size. Furthermore, the loss in pressure rise caused by the groove may actually be compensated by the diminished tip-leakage vortex and its blockage effect in the cascade passage. To address these issues thoroughly the problem can be treated in a constrained optimization framework.

E. Enhancement in Parallel Performance

The introduction of faster shared-memory and shared-distributed-memory machines like IBM Regatta P4 at Major Shared Resource Centers has motivated us to enhance the portability of the simulation code. The LES code is currently compatible with the SGI Orgin series, Compaq GS/ES series, SUN Enterprise series and IBM Regatta P4 without source level modifications. Separately from this, an MPI versions of the LES code are being implemented.

4. Significance to DoD

In liquid handling systems like turbomachinery pumps and submarine propulsors, the tip-leakage flow can induce cavitation, leading to strong acoustic noise, loss of performance, and structural damage. This complex, highly unsteady flow phenomenon is to date poorly understood and cannot be predicted by the traditional CFD method. The impact of the present LES work will be twofold: (1) the physical understanding gained from this study will be useful in predicting and eventually controlling cavitation, and (2) the highly efficient, parallel, generalized-coordinate LES code developed through this effort can be a useful tool for DoD's research and development community.

5. Systems Used

SGI Origin 3800 and IBM Regatta P4 (ARL MSRC)

6. CTA

CFD (Computational Fluid Dynamics)

7. References

[1]Wenger, C. W., Devenport, W. J., Wittmer, K. S., and Muthanna, C., "Two-Point Measurements in the Wake of a Compressor Cascade," *AIAA 98-2556.*

[2]Zierke, W. C., Farrel, K. J., and Straka, W. A., "Measurement of the Tip Clearance Flow for a High Reynolds-Number Axial-Flow Rotor," *Journal of Turbomachinery*, Vol. 119, 1997, pp. 1-8.

[3]Kameier, F., and Neise, W., "Experimental Study of Tip Clearance Losses and Noise in Axial Turbomachines and Their Reduction," *Journal of Turbomachinery*, Vol. 119, 1997, pp. 460-471.

[4]Muthanna, C., "Flowfield Downstream of a Compressor Cascade with Tip Leakage," Master Thesis, Department of Aerospace Engineering, Virginia Polytechnic Institute and State University, Feb., 1998.

[5]Muthanna, C., "The Effects of Free Stream Turbulence on the Flow Field Through a Compressor Cascade," Ph.D. Thesis, Department of Aerospace Engineering, Virginia Polytechnic Institute and State University, Feb., 2002.

[6]Wang, Y., "Tip Leakage Flow Downstream of a Compressor Cascade with Moving End Wall," Master Thesis, Department of Aerospace Engineering, Virginia Polytechnic Institute and State University, Feb., 2000.

[7]Khorrami, M. R., Li, F., and Choudhan, M., "Novel Approach for Reducing Rotor Tip-Clearance-Induced

Noise in Turbofan Engines," *AIAA Journal*, Vol. 40, 2002, pp. 1518-1528.

[8]Bae, J., Breuer, K. S., and Tan, C. S., "Control of Tip Clearance Flows in Axial Compressors," *AIAA 2000-2233*.

[9]Crook, A. J., Greitzer, E. M., Tan, C. S., Adamczyk, J. J., "Numerical Simulation of Compressor Endwall and Casing Treatment Flow Phenomena," *Journal of Turbomachinery*, Vol. 115, 1993, pp. 501-512.

[10]Kuhl, D. D., "Near Wall Investigation of Three Dimensional Turbulent Boundary Layers," Master Thesis, Department of Aerospace Engineering, Virginia Polytechnic Institute and State University, Aug., 2001.

[11]Senocak, I., "Computational Methodology for the Simulation of Turbulent Cavitating Flows," Ph.D. Thesis, Department of Mechanical Engineering, University of Florida, 2000.

[12]Arndt, R. E. A, "Cavitation in Fluid Machinery and Hydraulic Structures," Annual Review of Fluid Mechanics, Vol. 13, 1981, pp. 273-328.

[13]Joseph, D. D., "Cavitation and the State of Stress in a Flowing Liquid," *Journal of Fluid Mechanics*, Vol. 366, 1998, pp. 367-378.

[14]Knapp, R. T., Daily, J. W., and Hammitt, F. G., *Cavitation*, McGraw-Hill, 1970.

[15]You, D., Mittal, R., Wang, M., and Moin, P., "Study of Tip-Clearance Flow and Stator-Rotor Interaction Using Large-Eddy Simulation," 2002 DoD High Performance Computing Modernization Program Users Group Conference, Austin, Texas, June 10-14, 2002.

[16]You, D., Mittal, R., Wang, M., and Moin, P., "A Computational Methodology for Large-Eddy Simulation of Tip-Clearance Flows," *FEDSM 2003-45395*.

[17]You, D., Wang, M., Mittal, R., and Moin, P., "Study of Rotor Tip-Clearance Flow Using Large-Eddy Simulation," *AIAA 2003-0838*.

[18]Meneveau, C., Lund, T. S., and Cabot, W. H., "A Lagrangian Dynamic Subgrid-Scale Model of Turbulence," *Journal of Fluid Mechanics*, Vol. 319, 1996, pp. 233-242.

[19]Lund, T. S., Wu, X., and Squires, K. D., "Generation of Turbulent Inflow Data for Spatially-Developing Boundary Layer Simulations," *Journal of Computational Physics*, Vol. 140, 1998, pp. 233-258.

[20]Fadlun, E. A., Verzicco, R., Orlandi, P., and Mohd-Yusof, J., "Combined Immersed-Boundary Finite-Difference Methods for Three-Dimensional Complex Flow Simulations," *Journal of Computational Physics*, Vol. 161, 2000, pp. 35-60.

[21]Jeong, J., and Hussain, F., "On the Identification of a Vortex," *Journal of Fluid Mechanics*, Vol. 285, 1995, pp. 69-94.
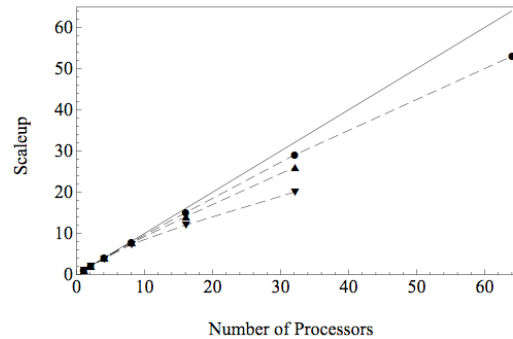
Figure 1: Parallel performance of the solver on various platforms. —, linear scaleup; -●-, SGI Origin 3800; -▲-, IBM Regatta P4; -▼-, Compaq GS320. The mesh size is $256 \times 256 \times 256$. Compaq GS320 and IBM Regatta P4 allow upto 32 CPU's while SGI Origin allows upto 512 CPU's for OpenMP parallelization.
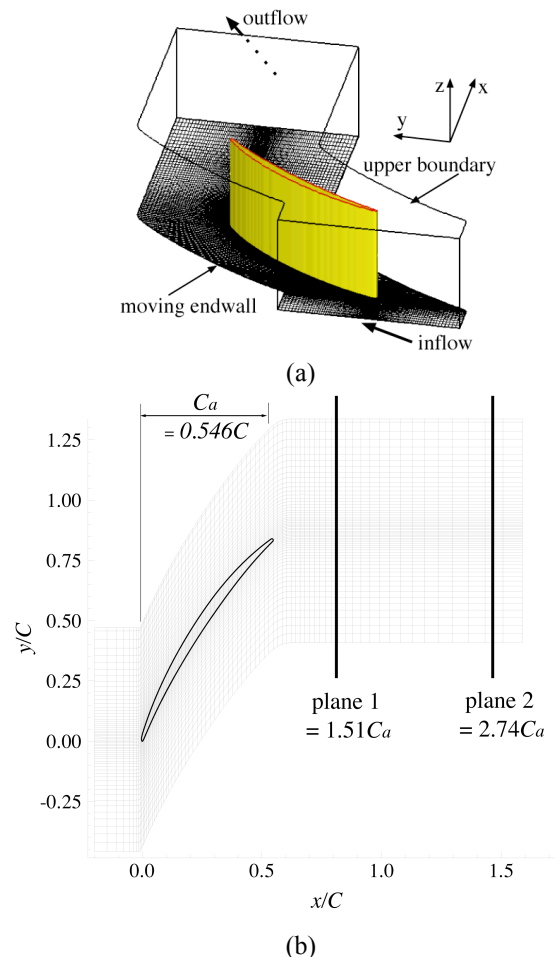
Figure 2: (a) Flow configuration and coordinate system; (b) computational domain and mesh in the *x-y* plane (1/6 lines plotted). The thick vertical lines represent measurement planes where comparisons are made between LES and experiment.[6]
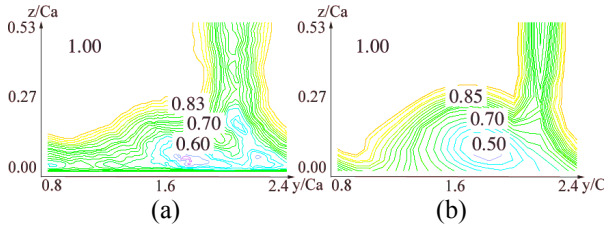
Figure 3: Comparison of mean streamwise velocity at x/Ca = 1.51. (a) LES; (b) experiment.[6] Contour levels are from 0.5 to 1.0 by 0.025.
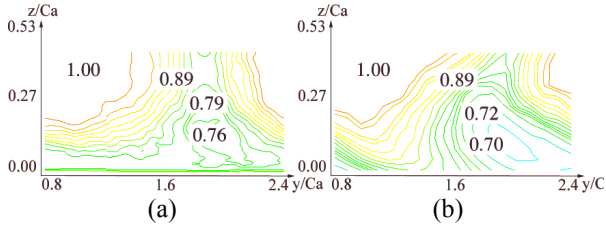
Figure 4: Comparison of mean streamwise velocity at x/Ca = 2.74. (a) LES; (b) experiment.[6] Contour levels are from 0.5 to 1.0 by 0.025.
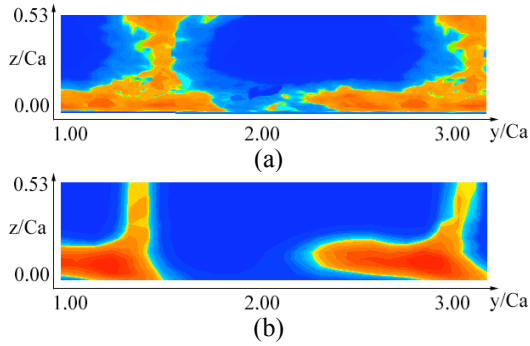
Figure 5: Comparison of Reynolds stress $v'v'$ at x/Ca = 1.51. (a) LES; (b) experiment.[6] Contour levels are from 0.003 to 0.012 by 0.0004.
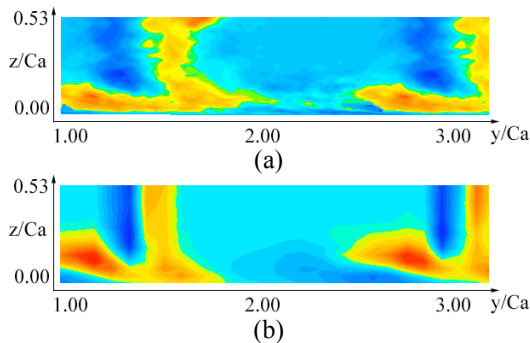
Figure 6: Comparison of Reynolds stress $u'v'$ at x/Ca = 1.51. (a) LES; (b) experiment.[6] Contour levels are from -0.004 to 0.004 by 0.0004.
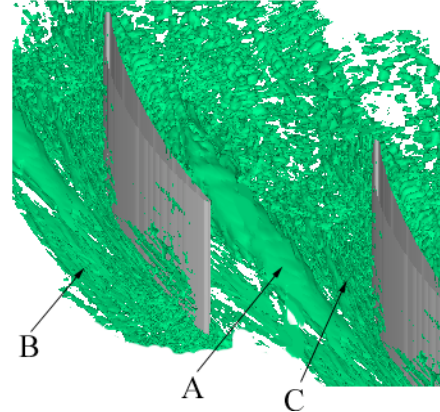
Figure 7: λ_2 iso-surfaces from time-averaged flowfield. A, B and C represent distinct vortical regions.
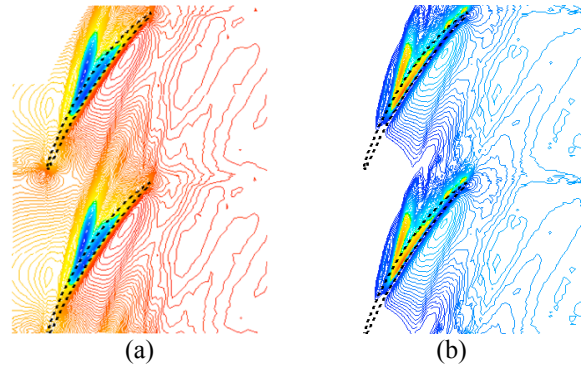
Figure 8: (a) Time-averaged pressure and (b) root mean square pressure fluctuation contours in an x-y plane at z/Ca = 0.0018. Contour levels are from -0.25 to 0.25 by 0.01 for (a) and from 0.0003 to 0.01 by 0.0005 for (b).
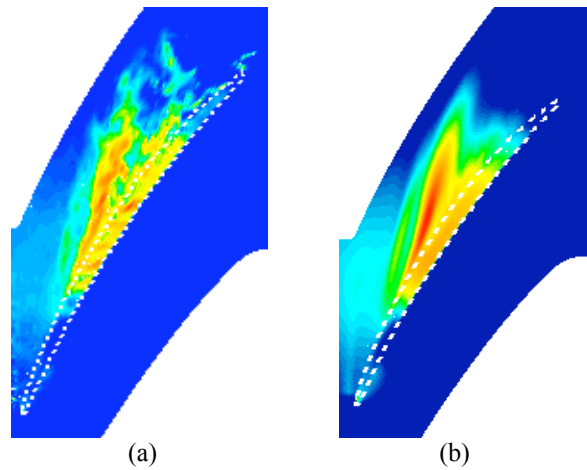
Figure 9: (a) Instantaneous and (b) time-averaged cavitation criterion, $B = 1/3(B_{11}+B_{22}+B_{33})$, contours in an x-y plane at z/Ca = 0.0018. Contour levels are from 0.03 to 0.3 by 0.05.

(a)

(b)

(c)
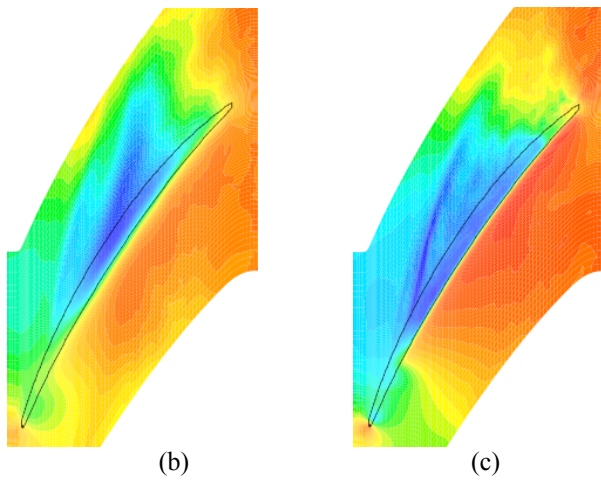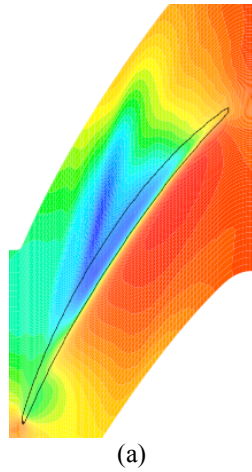
Figure 10: Contours of time-averaged pressure in an x-y planes at $z/Ca = 0.001$. Tip-gap sizes are (a) 0.0165, (b) 0.033 and (c) 0.00825. Contour levels are from -0.25 to 0.25 by 0.01.
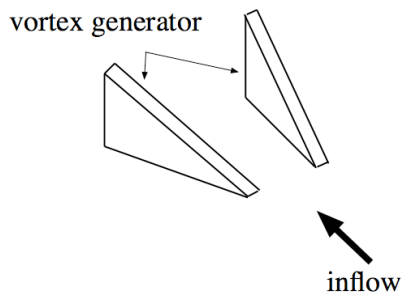
Figure 11: Configuration for LES of flow past a vortex-generator.
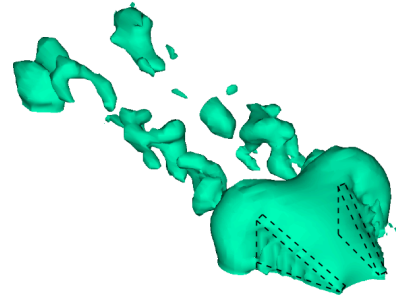
Figure 12: Iso-surface of instantaneous pressure ($p/\rho U_\infty^2 = -0.02$).
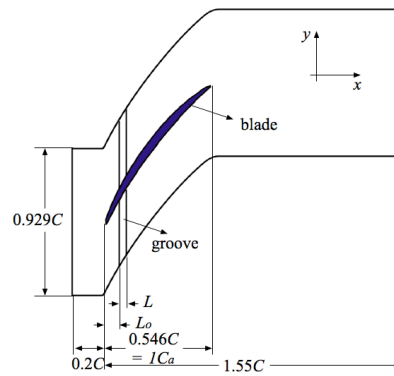
Figure 13: Schematic of the flow configuration with endwall groove, shown in the endwall (x-y) plane.

(a)

(b)
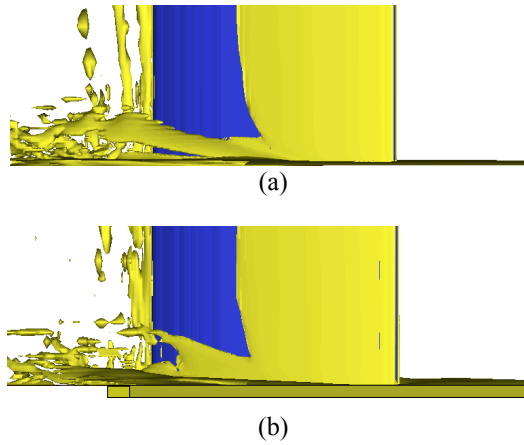
Figure 14: Iso-surfaces of instantaneous vorticity magnitude ($|\omega| = 10$). (a) Without endwall groove; (b) with endwall groove.